A R C H I V E S O F M E T A L L U R G Y A N D M A T E R I A L S
Volume 60 2015 Issue 3
DOI: 10.1515/amm-2015-0306

J. KOWALSKA*#, W. RATUSZEK*, M. WITKOWSKA*, A. ZIELIŃSKA-LIPIEC*, M. KOWALSKI**

MICROSTRUCTURE AND TEXTURE EVOLUTION DURING COLD-ROLLING IN THE Fe-23Mn-3Si-3Al ALLOY

ROZWÓJ MIKROSTRUKTURY I TEKSTURY W WALCOWANYM NA ZIMNO STOPIE Fe-23Mn-3Si-3Al

Fe–23wt.%Mn–3wt.%Si–3wt.%Al alloy was cast, homogenized at 1150°C, hot-rolled at temperatures between 1200°C and 900°C and next cold-rolled from 5% up to 40% reductions in thickness. Microstructure and texture of this alloy, which has a low stacking fault energy, were defined after cold-rolling. Investigation of transmission electron microscopy and X-ray diffraction showed that mechanical twinning and martensitic transformations ($\gamma_{fcc}\rightarrow\varepsilon_{hcp}$ and $\gamma_{fcc}\rightarrow\varepsilon_{hcp}\rightarrow\alpha'_{bcc}$) took place during cold-rolling. The crystallographic Shoji-Nishiyama (S-N) {00.2}ε‖{111}γ, <11.0>ε ‖ <110>γ and Kurdjumov-Sachs (K-S) {111}γ‖{101}α', <101>γ‖<111>α' relations between martensite (ε, α') and austenite (γ), were found in the cold-rolled material.

Keywords: Microstructure, Texture, Alloy, TRIP-effect, TWIP-effect

W artykule zamieszczono wyniki badań mikrostruktury i tekstury otrzymane dla stopu Fe–23%Mn–3%Si–3%Al (% masowe). Po odlaniu wlewek homogenizowano przy temperaturze 1150°C, walcowano na gorąco w zakresie temperatur 1200°C-900°C i następnie walcowano na zimno do odkształceń od 5% do 40%. Wyniki badań uzyskane przy użyciu transmisyjnej mikroskopii elektronowej i metod dyfrakcyjnych wskazują, że podczas odkształcenia plastycznego na zimno w stopie zachodzi mechaniczne bliźniakowanie i przemiana martenzytyczna. Występują zależności krystalograficzne pomiędzy austenitem (faza γ) i martenzytem (faza ε i faza α'), które opisują zależności: Shoji-Nishiyama {00.2}ε || {111}γ, <11.0>ε || <110>γ i Kurdjumowa-Sachsa {111}γ || {110}α, <110>γ || <111>α.

1. Introduction

High manganese austenitic steels constitute an attractive material for applications in the automotive industry. They exhibit a high strength and an exceptional plasticity. Those properties are obtainable in high-manganese steels in which plastic deformation induces martensitic transformation (the TRIP-effect) and mechanical twinning (the TWIP-effect). Those requirements could also be met by metastable austenitic chromium-nickel stainless steels during cold deformation [1-6]; however, that is infeasible due to economic reasons.

A stainless steel and high manganese steel are similar in that they both contain martensite ε and α'. In high manganese steel martensite ε, having a hexagonal structure is formed if the chemical composition of the steel is compatible with the formula: %Mn<33%Cx20, whereas α' martensite having a regular structure is formed if %Mn<22%Cx10.5 [7].

The Fe-Mn-C alloys have relatively low stacking-fault energies (SFE) [8]. Small values of SFE promote the dissociation of perfect dislocation into partials, which inhibits dislocation glide and activates different plasticity mechanisms [9]. The addition of Al and Si to the Fe-Mn alloys affects their stacking fault energies and phase stability, and it also gives rise to various properties of the Fe-Mn alloys such as strain hardening associated with deformation twinning, and strain-induced $\gamma_{fcc}\rightarrow\varepsilon_{hcp}$, $\gamma_{fcc}\rightarrow\varepsilon_{hcp}\rightarrow\alpha'_{bcc}$ and $\gamma_{fcc}\rightarrow\alpha'_{bcc}$ martensitic transformations. Al increases SFE and causes the suppression of the phase transformation. On the other hand, in the case of alloying by Si, the martensitic transformation is sustained [8, 10, 11]. With a decreasing value of SFE, plasticity is obtained by partial and perfect dislocation gliding, gliding and mechanical twinning, and gliding and martensitic transformation [9]. The formation of martensites: ε and α' depends on the chemical composition, temperature and the amount of strain. Some research has indicated that such alloys reveal mainly the TRIP-effect when the manganese contents are lower than 15%, while the TWIP-effect is dominant when manganese contents are higher than 25%. For manganese contents between 15% and 25%, both of the effects coexist [10, 12-15].

Most of the work devoted to high manganese steels has been concentrated on an alloy either is characterized by the TRIP, or by TWIP. In the present work, an alloy with the

* AGH UNIVERSITY OF SCIENCE AND TECHNOLOGY, FACULTY OF METALS ENGINEERING AND INDUSTRIAL COMPUTER SCIENCE, AL. A. MICKIEWICZA 30, 30-059 KRAKÓW, POLAND
** PEDAGOGICAL UNIVERSITY OF CRACOW, FACULTY OF MATHEMATICS, PHYSICAL AND TECHNICAL SCIENCE, POLAND
# Corresponding author: joannak@agh.edu.pl

manganese contents of 23% was designed to see if both the TRIP and TWIP effects could coexist.

An important aspect of the research is the determination of the texture of the material forming in the course of plastic deformation. In grains of certain crystallographic orientations, a phase transformation induced by deformation will occur more easily than in others (variant selection) [16-18].

2. Experimental procedure

The Fe-23Mn-3Si-3Al high manganese alloy was melted in a laboratory vacuum induction furnace. The chemical composition of the steel is given in Table 1.

After casting, the ingot was homogenized at 1150ºC for 3 hours under a protective argon atmosphere; next, it was hot-rolled at temperatures between 1200ºC and 900ºC to a plate with a thickness of 8 mm with reduction ratio of about 45%. Subsequently, the material was cold-rolled in a laboratory rolling mill at room temperature. Table 2 contains the degree of deformation and the number of passes of the samples taken for testing.

The deformed structure of the Fe-23Mn-3Si-3Al alloy was characterized using light microscopy (LM) on a Zeiss Axiovert 200MAT, and transmission electron microscopy (TEM) on a JEM 200CX. For optical observations, specimens were mechanically polished and etched with a 5% Nital solution. Specimens for TEM were mechanically fine-polished to a thickness of about 100 μm. 3-mm discs were then cut from the foils, and electrolytically-polished on twin-jet electropolishing equipment (Struers TenuPol-5 Controller Unit) at 10ºC using a solution containing CH_3COOH (90 vol. %) and $HClO_4$ (10 vol. %). Metallographic investigations were performed on longitudinal sections.

Microhardness of deformed specimens was measured on a Vickers INNOWA TEST microhardness tester with 1 Newton of load on electrolitically-polished surfaces.

X-ray investigations, including phase analysis and texture measurement from the central layers of the sheets, were conducted on a Siemens D500 and Bruker D8 Advance diffractometers using $Cu_{K\alpha}$ and $Co_{K\alpha}$ radiation. Samples after hot-rolling (0%) and cold-rolling (5%-40%) were ground on 2000 grit papers. Subsequently, the samples were electrolytically-polished to remove the martensite induced during sample preparation.

3. Results and discussion

In the initial state (0% − after hot-rolling), a fully austenitic microstructure was observed by light microscopy. Variation in grain size is caused by recrystallization occurring after hot-rolling (Figure 1a); recrystallization twins are visible. The effects of deformation include intersecting deformation bands, which shows that plastic deformation occurs in various systems (Figure 1b-c). These are preferential sites for the formation of the martensitic phase [19].

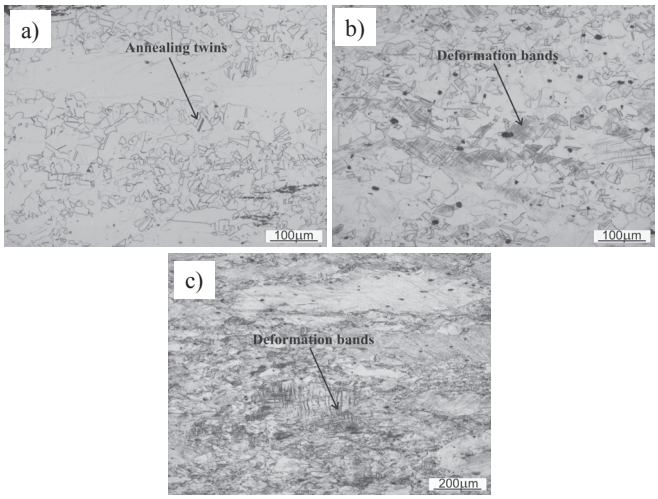

Fig. 1. Microstructure of Fe-23Mn-3Si-3Al alloy (a) in the initial state, after deformation (b) 5%, (c) 30% - light microscopy

After 5% deformation, transmission electron microscopy revealed numerous stacking faults (Figure 2a) which, it has been shown [8, 15, 20], assist nucleation of a hexagonal phase (martensite ε). Reflections of the ε phase were observed on the diffractogram (Figure 2b). Increased deformation apart from phase transformation γ→ε (Figure 3a-b) results in a change of the deformation mechanism; numerous deformation microtwins and shear bands were noticed (Figure 3c-d). In these areas martensite α' was detected by dark field microscopy (Figure 3c-d). After 20 and 30% deformation, both martensites: ε and α', are observed, which indicates that a phase transformation occurs in the following way: γ→ε and γ→ε→α' (Figure 3 and 4).

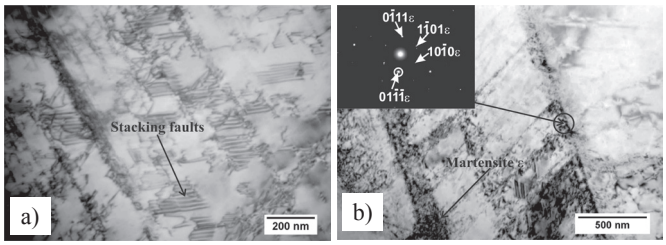

Fig. 2. TEM micrographs of Fe-23Mn-3Si-3Al alloy after 5% cold-rolling and SADPs taken from areas indicated by a circle (a) BF, (b) BF, diffraction pattern $[1\bar{2}1\bar{3}]\varepsilon$

TABLE 1

Chemical composition of Fe-23Mn-3Si-3Al alloy (wt. %)

Mn	Si	Al	C	Fe
22.96	2.85	2.66	0.065	balance

TABLE 2

Total engineering values (ε) and logarithmic values (δ), the number of passes during cold-rolling and deformation per pass in the Fe-23Mn-3Si-3Al alloy

ε [%]	5	10	20	30	40
δ	0.06	0.10	0.22	0.39	0.50
No. passes	4	7	10	14	18
Deformation per pass [%]	0.015	0.014	0.022	0.027	0.027

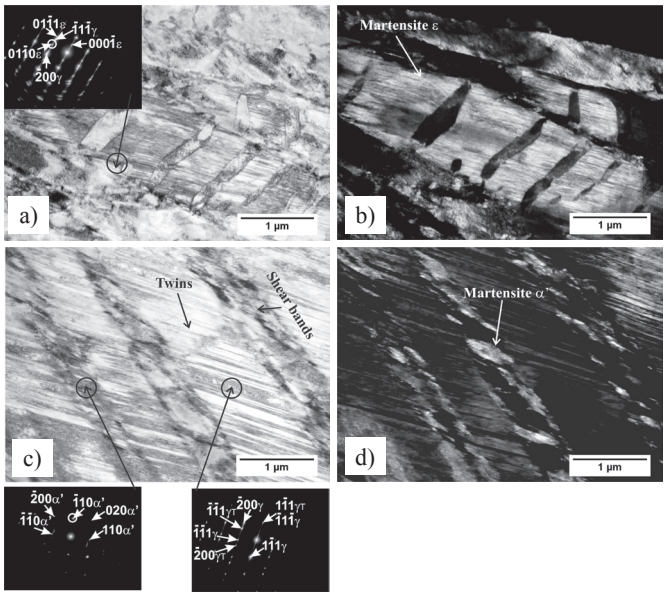

Fig. 3 TEM micrographs of Fe-23Mn-3Si-3Al alloy after 20% cold-rolling and SADPs taken from areas indicated by a circle (a) BF, diffraction patterns $[2\bar{1}\bar{1}0]\varepsilon \| [011]_\gamma$, (b) DF with $(01\bar{1}0)\varepsilon$, (c) BF, diffraction patterns $[001]\alpha'$ and $[011]\gamma \| [011]_T$, (d) DF with $(\bar{1}10)\alpha'$

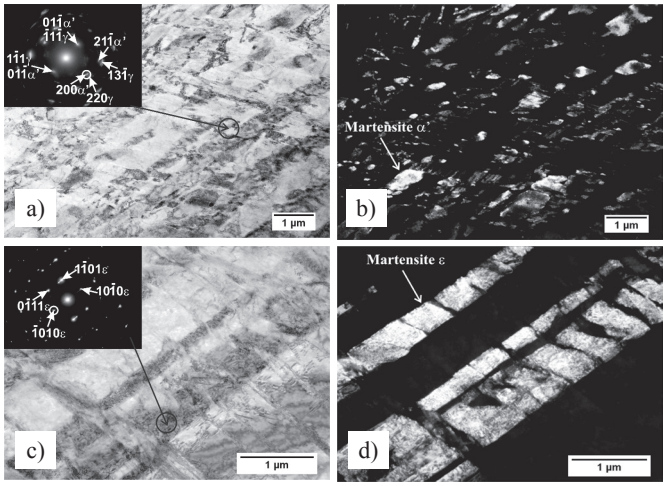

Fig. 4. TEM micrographs of Fe-23Mn-3Si-3Al alloy after 30% cold-rolling and SADPs taken from areas indicated by a circle (a) BF, diffraction pattern $[011]\alpha' \| [\bar{1}12]\gamma$, (b) DF with $(200)\alpha'$, (c) BF, diffraction pattern $[1\bar{2}\bar{1}\bar{3}]\varepsilon$, (d) DF with $(\bar{1}010)\varepsilon$

With an increase in deformation, microhardness increases (Figure 5), which results from the refinement of the structure as a result of twinning and formation of the hard martensistic phase.

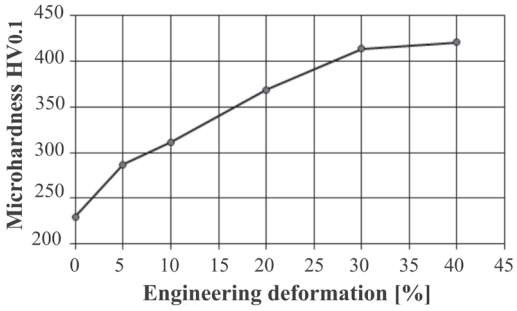

Fig. 5. Changes of microhardness after deformation

X-ray diffraction results are presented in Figures 6-10. The pattern of the high manganese steel after annealing and hot-rolling (0%) shows that the material has an austenitic structure (γ), as diffraction lines originating from γ-phase only are observed. The peak manifesting the greatest intensity is 111γ, accompanied by the weaker: 220γ, 200γ, 311γ and 222γ (Figure 6). For the sample after 5% deformation, very weak peaks originating from ε martensite, having a hexagonal close-packed (HCP) structure, 10.1ε, 10.2ε, and α' martensite, having body-centered cubic (BCC) structure, 200α' and 211α' (Figure 6) appear. After 10% deformation, an increase in the intensity of diffraction lines originating from the α'-phase (110α', 200α' and 211α') (Figure 6) is observed. After 20% deformation, an increase in the intensity of the 10.1ε peak was detected, and, after further deformation, it became weaker. The X-ray results confirm earlier transmission electron microscopy observations (Figures 2-4).

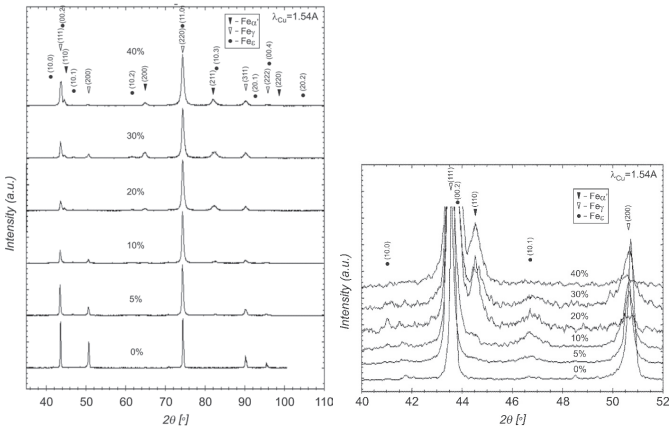

Fig. 6. X-ray diffractions patterns of the Fe-23Mn-3Si-3Al alloy in the initial state (0%) and after cold-rolling to reductions 5%-40% (a), the expanded plot the (111) and (200) for austenite (γ) and the (002) and (101) for martensite ε peaks (b).

In order to analyse the texture, four pole figures of the planes were measured: {111}γ, {200}γ, {220}γ, {311}γ for austenite, five pole figures (10.0)ε, (00.2)ε, (10.1)ε, (10.2)ε, (20.1)ε for martensite ε, and three pole figures {110}α', {200}α', {211}α' for martensite α'. On the basis of the experimental pole figures, full pole figures and the orientation distribution function (ODF) were calculated. ODF at the cross-section: $\varphi_2=0^o$, pole figure 111γ for austenite, and 00.2ε and 110α' for martensites: ε and α' (Figures 7, 9), respectively, are presented.

Austenite in the initial state was characterized by a comparatively strong texture. The maximum value of the orientation distribution function (ODF) matched the Goss orientation {110}<001> situated in the non-limited fibre α=<110>‖ND. In the texture of austenite, weak orientations such as {110}<112> and {110}<110> (Figure 7) are also observed. For deformations 5 to 20%, the degree of texturing of austenite increases. Orientations included in the fibre α=<110>‖ND are strengthened. After 5% deformation, a weak component appears in the texture {113}<332>. After 10% deformation, the maximum of intensity of ODF was relocated from the Goss orientation {110}<001> to orientation {110}<115> (Figure 7). Increase in the deformation up to 30% results in a weakening of the texture of austenite, which

is connected with the martensitic transformation induced by deformation $\gamma_{fcc} \rightarrow \varepsilon_{hcp}$ and $\gamma_{fcc} \rightarrow \varepsilon_{hcp} \rightarrow \alpha'_{bcc}$, confirmed by diffractograms (Figure 6). For deformations between 10 and 30%, a phase transformation results in the formation of both martensites ε, and α'. Strengthening of the texture of austenite after 40% due to an increase in the degree of plastic deformation austenite grains remained after the martensitic transformation (Figure 7). In this range of deformation is not observed transformation $\gamma \rightarrow \varepsilon$ only $\varepsilon_{hcp} \rightarrow \alpha_{bcc}'$. This is confirmed by the lack of peak from ε phase on the diffractogram of the alloy after 40% deformation (Figure 6). After 40% deformation, the maximum value of ODF for austenite matches the following orientation: {110}<755> (Figure 7).

Within the texture of deformed austenite there is a number of twin orientations. For example, figure 8 shows transformation of the ideal {110}<001> orientation carried out by rotation around <111> axes by an angle $(2n-1)x60^o$. This transformation confirms the presence of the orientation {110}<001> and the {110}<221> twin orientation within the texture of deformed austenite as well as a weaker component {114}<221>.

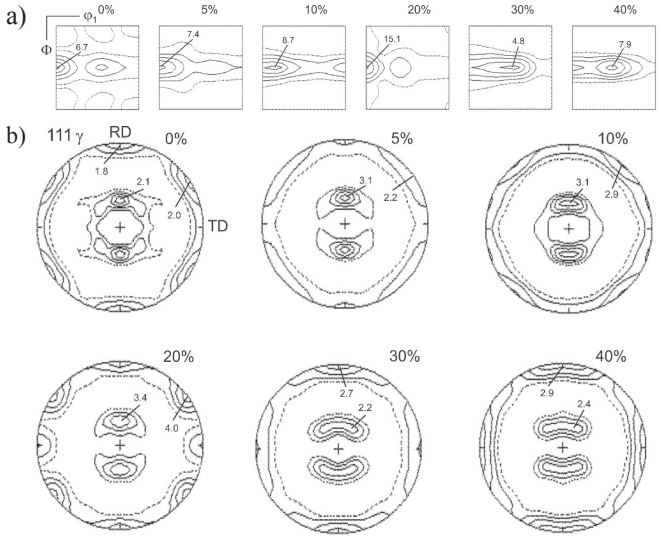

Fig. 7. Orientation distribution functions (ODF's) in section $\varphi_2=0^o$ (a) and calculated pole figure 111γ (b) for austenite in the initial state (0%) and after cold-rolling to reductions 5%-40%

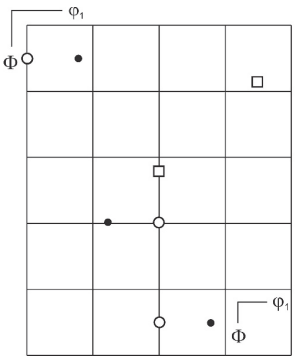

Rotation	Final orientation	Symbol
$1\bar{1}1$	$(\bar{1}\bar{1}0)[2\bar{2}\bar{1}]$	•
$\bar{1}1\bar{1}$	$(\bar{1}\bar{1}0)[2\bar{2}\bar{1}]$	•
$11\bar{1}$	$(11\bar{4})[\bar{2}\bar{2}\bar{1}]$	□
$\bar{1}\bar{1}1$	$(11\bar{4})[\bar{2}\bar{2}\bar{1}]$	□
$\bar{1}11$	$(\bar{1}\bar{1}0)[\bar{2}2\bar{1}]$	•
$1\bar{1}\bar{1}$	$(\bar{1}\bar{1}0)[\bar{2}2\bar{1}]$	•
111	$(114)[22\bar{1}]$	□
$\bar{1}\bar{1}\bar{1}$	$(114)[22\bar{1}]$	□
Ideal orientation {110}<001>		o

Fig. 8. Transformation of the ideal {110}<001> orientation in the austenite texture according to $(2n-1)x60^o$ <111> rotation (section $\varphi_2=0^o$).

In Figure 9a, the calculated pole figures of the planes 00.2ε for martensite having a hexagonal structure for 5, 10 and 20% deformations are presented. After 5% deformation, the texture of ε martensite is clear and with the maximum situated at the distance of approximately 32^o from ND and matching the orientation (10.3). Together with an increase in deformation, a non-significant weakening of the main constituents of the texture of ε martensite is observed. After 20% deformation, on the pole figure 00.2ε a division of the maximum into two symmetrical ones is observed. Additionally, constituents situated at the distance of approximately 12^o and 55^o from RD in the direction of TD appear (Figure 9a). For higher deformations 30% and 40%, it proved impossible to measure the texture of ε martensite, which is connected with a small volume contribution of this phase.

For the initial state and small degrees of deformation (0% and 5%), the texture was not measured, because the contribution of the magnetic phase (α') was small, and no clear diffraction lines were observed (Figure 6). It is only after 10% deformation that clear diffraction lines appear. Figure 9b presents the texture for α' martensite (pole figures 110). The texture of α' martensite for all deformations is comparatively weak, and has a partly-fibrous character.

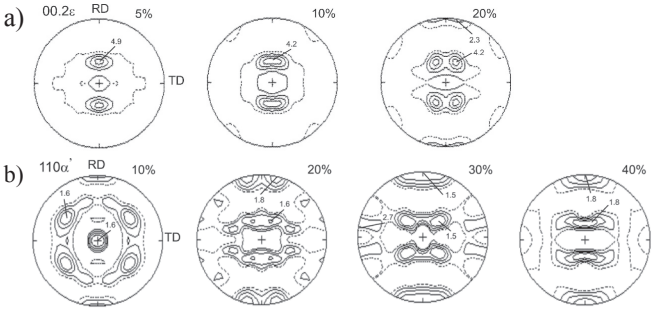

Fig. 9. Calculated pole figure (a) 00.2ε for ε martensite after cold-rolling 5%-20% (b) 110α' for α' martensite after cold-rolling 10%-40%

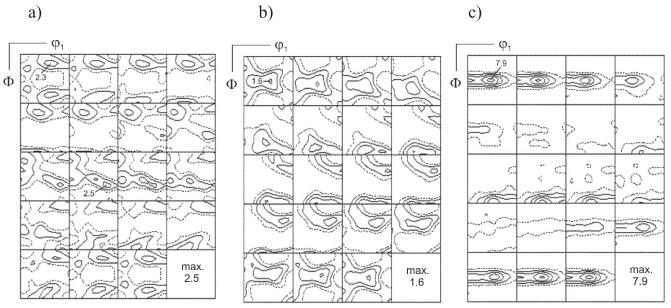

Fig. 10. Experimental orientation distribution functions (ODF's) for (a) α' martensite after 40% deformation, (b) for austenite which was transformed with α' to γ according relation K-S and (c) for austenite after 40% deformation

Analysing the pole figures of the planes (111)γ and (00.2)ε for the material after 5 and 10% deformation, it was ascertained that there occur crystallographic relations between the phases (Figures 7b and 9a). The best description of this correlation was provided by a relation first observed in cobalt by Burgers [21], and based mainly upon geometrical analysis. He reported the following crystallographic relation between the face-centred cubic (FCC) and the hexagonal close-packed

(HCP) phases: $(111)\gamma \| (0001)\varepsilon$. He determined that the transformation consists of glide on every other plane in the direction $[11\bar{2}]$. Afterwards, Paar [21], analysing the X-ray diffraction pattern of the polycrystal sample of manganese steel, provided the correlation $(111)\gamma \| (0001)\varepsilon$ and $[1\bar{1}0]\gamma \| [1\bar{2}10]\varepsilon$. Currently, that relation is also known as the Shoji-Nishiyama relation (S-N) $\{00.2\}\varepsilon \| \{111\}\gamma$ and $<11.0>\varepsilon \| <110>\gamma$ [22]. The existence of this relationship is also confirmed by the observations of the microstructure after 20% deformation (Figure 3c-d). Similar crystallographic relations were observed in high manganese steel also by others [7, 13, 20, 23]. In the material after 40% deformation, the crystallographic relations between austenite (γ) and martensite α' having a body-centred cubic structure (BCC) can be described by the Kurdjumov-Sachs relation (K-S) $\{111\}\gamma \| \{101\}\alpha$' and $<101>\gamma \| <111>\alpha$' (Figures 7b and 9b). Transformation of the experimental orientation distribution function for martensite α' after 40% deformation was performed in accord with the K-S relation (Figure 10). Comparing the results of the texture of austenite obtained after transformation (Figure 10b) with the results of experiments (Figure 10c) indicates a good compatibility of the main components. The occurring differences result from the fact that the transformations were performed without variant selection.

4. Conclusions

1. In the entire range of deformations, a number of processes occur, namely: the deformation of austenite, dislocation glide, phase transformation $\gamma_{fcc} \rightarrow \varepsilon_{hcp}$, $\gamma_{fcc} \rightarrow \varepsilon_{hcp} \rightarrow \alpha'_{bcc}$, and twinning induced by deformation, and also the deformation of the formed martensites (ε and α'), and that their contributions is changing.
2. For the small amounts of deformation, numerous stacking faults occur, on which hexagonal phase nucleates (ε). In the case of larger deformations, the mechanism changes to twinning, and also the following transformation: $\varepsilon_{hcp} \rightarrow \alpha'_{bcc}$, occurs.
3. In the texture of a deformed austenite, orientations which dominate are those included in the fibre: α=**<110>** $\|$ ND. The relocation of the ODF maximum from the close orientation of the alloy $\{110\}<112>$ to the Goss orientation $\{110\}<001>$ for 20% deformation is connected with shear bands formed in the structure. Weakening the texture for 30% deformation is connected with the transformation of austenite into martensite.
4. Between austenite (γ) and martensite (ε and α'), crystallographic correlations are described by the Shoji-Nishiyama relations (S-N) $\{00.2\}\varepsilon \| \{111\}\gamma$ and $<11.0>\varepsilon \| <110>\gamma$, and also Kurdjumov-Sachs (K-S) $\{111\}\gamma \| \{101\}\alpha$' and $<101>\gamma \| <111>\alpha$'.

Acknowledgements

This work was sponsored by the Polish National Science Centre under Contract no 2011/01/D/ST8/03905.

Appreciation is also expressed to Prof. A.S. Wronski (University of Bradford, UK) who edited the text.

REFERENCES

[1] E. Nagy, V. Martinger, F. Tranata, J. Sólyom, Deformation Induced Martenstic Transformation in Stainless Steel, Mater. Sci. Eng. **A378**, 308-331 (2004).

[2] T. Suzuki, H. Kojima, K. Suzuki, T. Hashimoto, S. Koike, M. Ichihara, Plastic Deformation and Martensitic Transformation in an Iron-Base Alloy, Scripta Metall. **10**, 4, 353-358 (1976).

[3] S.M. Tavares, D. Gunderov, V. Stolyarov, J.M. Neto, Phase Induced by Severe Plastic Deformation in the AISI 304L Stainless Steel, Mater. Sci. Eng. **A358**, 32-36 (2003).

[4] H. Oettel, U. Martin, The nature of the TRIP-effect in metastable austenitic steels Int. J. Res. **97**, 12, 1642-1647 (2006).

[5] W. Ratuszek, J. Kowalska, A. Bunsch, M. Rumiński, A. Zielińska–Lipiec, Development of deformation texture of austenitic steel wires, Arch. Metall. Mater. **53**, 1, 167-174 (2008).

[6] A. Bunsch, J. Kowalska, K. Chruściel, Texture and Microstructure of Annealed AISI302 Steels Wires, Arch. Metall. Mater. **53**, 1, 125-130 (2008).

[7] Y. Lü, B. Hutchinson, D.A. Molodov, G. Gottstein, Effect of Deformation and Annealing on the Formation of ε-martensite in an Fe-M-C alloy, Acta Mater. **58**, 3079-3090 (2010).

[8] H. Ding, H. Ding, D. Song, Z. Tang, P. Yang, Strain Hardening Behavior of TRIP/TWIP Steel with 18.8% Mn, Mater. Sci. Eng. **A528**, 868-873 (2011).

[9] J. A. Jimenez, G. Frommeyer, Analysis of the microstructure evolution during tensile testing at room temperature of high-manganese austenitic steel, Mater. Charact. **62**, 221-226 (2010).

[10] O. Grässel, L. Krüger, G. Frommeyer, L.W. Meyer, High Strength Fe-Mn-(Al, Si) TRIP/TWIP Steels Development - Properties – Application, International Journal of Plasticity, **16**, 1391-1409 (2000).

[11] A.S. Hamada, L.P. Karjalainen, M.C. Somani, The Influence of Aluminium on Hot Deformation Behavior and Tensile Properties of High-Mn TWIP Steels, Materials Science and Engineering **A467**, 114-124 (2007).

[12] G. Frommeyer, U. Brüx, P. Neumann, Supra-Ductile and High-Strength Manganese-TRIP/TWIP Steels for High Energy Absorption Purposes, ISIJ International, **43**, 3, 438-446 (2003).

[13] J. Kowalska, W. Ratuszek. M. Witkowska, A. Zielińska–Lipiec, Development of Microstructure and Texture in Fe-26Mn-3Si-3Al Alloy During Cold-Rolling and Annealing, J. Alloys Comp. vol. **615 Suppl. 1**, S583–S586 (2014).

[14] J.-B. Seol, J.E. Jung, Y.W. Jang, C.G. Park, Influence of Carbon Content on the Microstructure, Martensitic Transformation and Mechanical Properties in Austenite/ε-Martensite Dual-Phase Fe-Mn-C Steels, Acta Mater. **61** 558-578 (2013).

[15] H. Idrissi, K. Renard, L. Rueland, D. Schyvers, P.J. Jacques, On the Mechanism of Twin Formation in Fe-Mn-C TWIP Steels, Acta Mater. **58** 2464-2476 (2010).

[16] C. Hyoung Cheol., S. Hong Chul, C. Young Won, The Formation Kinetics of Deformation Twin and Deformation Induced ε-Martensite in an Austenitic Fe-C-Mn Steel, Scripta Mater. **40**, 1171-1177 (1999)

[17] X. Liang, X. Wang, H.S. Zurob, Microstructural Characterizationof Transformable Fe-Mn Alloys at Diffrent Lenght Scales, Mater. Charact. **60**, 1224-1231 (2009).

[18] E.P. Kwon, S. Fujieda, K. Shinoda, S. Suzuki, Texture Evaluation and fcc/hcp Transformation in Fe-Mn-Si-Cr Alloys by Tensile Deformation, Mater. Sci. and Eng. **A527**, 6524-6532 (2010).

[19] A.F. Padilha, R.L. Plaut, P.R. RIos, Annealing of Cold-Worked Austenitic Stainless Steel, ISIJ International **43**, 2, 135-143 (2003).

[20] L. Bracke, G. Mertens, J. Penning, B. DeCooman, M. Liebeherr, N. Akdut, Influence of Phase Transformations on the Mechanical Properties of High-Strength Austenitic Fe-Mn-Cr Steel, Metall. Mater. Trans. A, **37A**, 307-317 (2006).

[21] S. Gorczyca, Phase Transformation $\varepsilon \rightarrow \gamma$ ac a Process Previous to the Recrystallization of Cold Worked Chromium-Manganese Austenitic Steel, Scentific books of AGH University of Science and Technology, No.**187**, Kraków (1967).

[22] W. Zhang, Z. LIu, Z. Zhang, G. Wang, The Crystallographic Mechanism for Deformation Induced Martensitic Transformation Observed by High Resolution Transmission Electron Microscope, Materials Letters **91**, 158-160 (2013).

[23] F. Lu, P. Yang, L. Meng, F. Cui, H. Ding, Influence of Thermal Martensite and Grain Orientation on Strain-Induced Martensites in High Manganese TRIP/TWIP Steels, J. Mater. Sci. Technol. **27** (3), 257-265 (2011).

Received: 20 October 2014.